論文 / 著書情報
Article / Book Information

Title	Nonlinear normal modes and localization in two bubble oscillators
Author(s)	Naohiro Sugita, Toshihiko Sugiura
Citation	Ultrasonics, Vol. 74, pp. 174-185
Pub. date	2016, 10
DOI	http://dx.doi.org/10.1016/j.ultras.2016.10.008
Creative Commons	See next page.
Note	This file is author (final) version.

License

Nonlinear normal modes and localization in two bubble oscillators

Naohiro Suigta[a], Toshihiko Sugiura[a,*]

[a]*Department of Mechnical Engineering, Keio University, Yokohama 2238522, Japan*

Abstract

We investigated a bifurcation structure of coupled nonlinear oscillation of two spherical gas bubbles subject to a stationary sound field by means of nonlinear modal analysis. The goal of this paper is to describe an energy localization phenomenon of coupled two-bubble oscillators which occurs as a result of internal resonance between the two bubble oscillation, leading to bifurcations of the steady-state oscillation amplitudes. Approximate asymptotic solutions of nonlinear normal modes (NNMs) and a steady state solution are obtained based on the method of multiple scales. It is found that localized oscillation takes on in a neighborhood of the localized in-phase oscillation mode. The analytical solutions of the amplitude and the phase shift of the steady-state oscillation are compared with numerical results and found to be in good agreement within the limit of small-amplitude oscillation. For larger amplitude oscillation, a bifurcation diagram of the localized solution as a function of the driving frequency and the separation distance between the bubbles is provided in a presence of the thermal damping. The obtained results show that the localized oscillation can occur for a fairly typical parameter range used in practical experiments and simulations in the early literatures.

Keywords: Bubble dynamics, Coupled nonlinear oscillation, Nonlinear localization, Bifurcation, Nonlinear normal modes, Perturbation analysis

1. Introduction

Small cavitation bubbles repeatedly change their volume in an oscillating pressure field without losing their spherical symmetry. Such continuous response of the oscillating bubbles is referred to as stable acoustic cavitation[1], which is employed in many engineering applications such as ultrasonic cleaning[2], ultrasound imaging[3, 4] and therapy[5]. The interactions between sound and cavitation bubbles have been extensively studied because the resonant phenomenon of the bubble oscillation is an important mechanism of the above applications.

The external acoustical energy is continuously localized to the oscillating bubble and subsequently released to surroundings as the secondary radiation pressure which, in turn, drive the neighboring bubbles, leading to the mutual interaction of the oscillating bubbles. We can consider the bubbles as nonlinear oscillators coupled by the radiation pressure, and readily analyze the motion of the bubble walls on the basis of fairly mathematical treatments: that is to say the spherical dynamics of bubbles with time-varying radii $R_i(t)$. As the dynamical behavior of the bubble population is practically of importance to improve the validity of ultrasonic techniques, the coupled oscillation of resonant bubbles has been studied intensively for many years.

At the outset of the theoretical studies on the coupled bubble oscillation, solid mathematical consequences have been offered by linear modal analyses[6, 7]. Zabolotskaya analyzed linear normal modes (LNMs) of two gas bubbles pulsating in a liquid using the Lagrangian formalism, and showed that the linear normal frequencies depends on the separation distance between the two bubbles[6]. Takahira provided a general

*Corresponding author
Email address: sugiura@mech.keio.ac.jp (Toshihiko Sugiura)

derivation of coupled N bubble dynamics accounting for the translational motion and deformation of the bubbles on a basis of the potential solution. The resulting eigenvalue problem concluded that the frequency of the fundamental normal mode is much smaller than that of an unbounded single bubble[7]. However, in contrast to linear systems, extremely complex behaviors are encountered in nonlinear systems[8]. Although nonlinear spherical dynamics of a single bubble and its bifurcation structure, including subharmonic generation, period-doubling bifurcation and chaotic oscillation, have been explored[34], little is known about the bifurcation structures of the coupled bubble dynamics, and most of the studies have been employed numerical techniques[9, 10, 11, 12, 13].

The numerical study of Takahira demonstrated the period-doubling bifurcation and accompanying chaotic oscillation of interacting multi-bubble systems[9]. The fundamental feature identified in the analysis is that equal-sized bubbles with the same initial radii arranged in a symmetrical configuration all take on the same behavior similar to that of an unbounded bubble, whereas cluster bubbles with different initial equilibrium radii cannot oscillate independently from one another but experience a collective behavior. Macdonald also reported numerical results on the same collective behavior in multi-bubble interactions of ultrasound contrast agent microbubbles[10].

Herein, we particularly focus on nonlinear localization[8] of the mutual bubble interaction in which the total vibrational energy of the system is confined to some bubbles due to the nonlinearity of the bubble oscillation even though they are equally-sized and arranged in a symmetric configuration. This symmetry breaking property is one of the distinctive feature of the localized oscillation[14, 15] considered in this study. This symmetrical arrangements and equal-sized assumption have been used in numerical investigation of the effects of bubble sizes and spatial arrangement on the coupled bubble dynamics[11, 12, 13, 16]. However, the fundamental bifurcation structure of the coupled bubble dynamics has not been addressed because most of the above studies are based on numerical investigation.

The linear modal analyses have been definitely powerful tools for interpreting the underlying linear system. However, they are still inadequate to properly describe complicated nonlinear phenomena. In order to make a general survey of the bifurcation structure of the coupled bubble dynamics, analytical investigation of nonlinear normal modes (NNMs)[8, 14] is an essential approach to a greater insight on the structural nature of the multi-bubble dynamics. At the first attempt of NNMs, Rosenberg extended straightforwardly the concept of LNMs to nonlinear vibration systems and defined an NNM as a vibration *in unison* where all mass points in the system display periodic motions with the same period[17, 18, 19]. In the definition, all displacements pass through their equilibrium points and reach their extreme values simultaneously. It should be also noted that NNMs inherit the invariance property of LNMs (i.e., motions that depart from the NNM confined in it for all time), which is exploited to derive the NNMs in the perturbation analysis of this study.

There have been a few studies which used a perturbative method to obtain the steady-state solution of bubble oscillation. Prosperetti presented a second order steady-state solution of Rayleigh's equation of motion for the bubble wall by means of an asymptotic expansion method[20]. The analytical results enabled it evident to predict the multivalued solution of the nonlinear oscillation and the unstable region of subharmonic resonance as well as their hysteresis behavior. Francescutto used an asymptotic method of multiple scales to obtained explicit and simpler formulas for the second order approximate solution[21]. Nevertheless, since these results are for a single bubble, nonlinear resonance of the vibration modes among multiple bubbles are still unclear. We employ the method of multiple scales[22, 23] to derive NNMs of the coupled bubble oscillation and investigate the internal resonance[22] of the steady-state amplitude and the phase shift.

In the present study, we will restrict the analysis to a resonant pair of two bubbles. In order not to limit the generality, the bubble sizes are allowed to be different in the perturbation analysis (Section 3), but assumed to be similar so that the two uncoupled natural frequencies of isolated bubbles have a slight difference by the order of $O(\epsilon^2)$ where ϵ is a nondimensional oscillation amplitude. Since the aim of this paper is to investigate the bifurcation structure of the radial dynamics of a resonant pair of bubbles, the separation distance of the bubbles is assumed to be unchanged by the translational instability due to Bjerknes forces though it is important to account for the transient response and hysteresis property for a full understanding of the bubble structure dynamics[24]. The circumstances of a fixed bubble distance is not improbable but

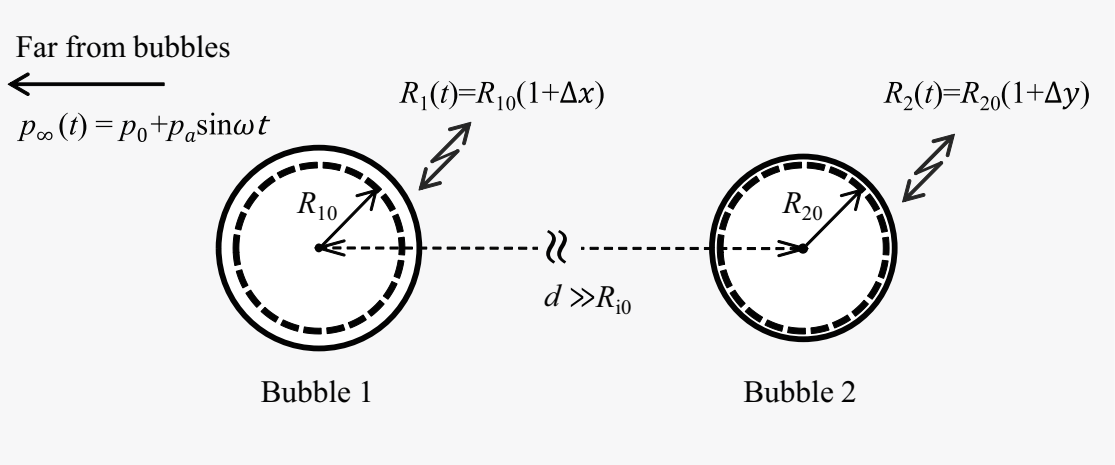

Figure 1: A schematic model of two oscillating bubbles.

achieved in the case of surface cavitation bubbles attached on a solid surface[25, 26]. Because of the adhesion between the bubble and wall surface the bubble mobility is decreased, and the bubble distances tends to remain almost fixed. Additionally, the effect of the wall boundary is replaced with a mirror image of the real bubble. This allows the dynamics of the hemispherical bubble to be well described by the Rayleigh-Plesset equation for a spherical bubble in an unbounded space.

In Section 2, the equations of radial motion for the coupled dynamics of two spherical gas bubbles are presented, and the linear theory is summarized to illustrate the basic concept of normal modes. Perturbation analysis in Section 3 provides the approximate solution of the steady-state oscillation, and the NNMs of the two-bubble system are developed from the perturbation solution obtained. Section 4 performs numerical calculations for large amplitude oscillation in a broader range of parameter spaces. Important findings and conclusions are summarized in Section 5.

2. Radial dynamics of two spherical bubbles

We consider two gas bubbles separated by a fixed distance in a liquid driven by a stationary sound field sketched in Fig. 1. The wave length is assumed larger enough for the two bubbles to experience the equal driving pressure. Bubble oscillations are inertially controlled by the periodic pressure change in the far field, and develop a secondary sound field without distorting each others sphericity. The radiation pressure induced by one of the bubbles, bubble 1, measured at the center of the other bubble, bubble 2, is

$$p_r = \frac{\rho}{4\pi d}\frac{d^2V_1(t)}{dt^2} \tag{1}$$

where V_1 is the time-varying volume of bubble 1, d is the separation distance between the bubble centers which is enough larger than the wave length for the bubbles to remain spherical with the time-varing radii $R_1(t)$ and $R_2(t)$, respectively during oscillation. Eq. (1) is exerted on the neighboring bubbles as an additional driving pressure, and their resulting spherical dynamics are coupled with each other.

Herein, the liquid is assumed to be cold, and the vapor pressure is omitted from the bubble contents, while the linear thermal damping[27, 28] was used in the numerical simulation (Section 4) in order to account for the thermal behavior of gas in the bubble. Shape and dissolution instabilities[29] are neglected although they are generally needed to account for lifetimes of oscillating cavitation bubbles. The fission[30] phenomenon and rectified diffusion[31] are also not taken into account because the scope of this study is to identify the bifurcation structure of the spherical bubble oscillators.

2.1. Equations of radial motion

For spherical dynamics of an oscillating bubble of radius $R_i(t)$, we use a modified form of the coupled Keller-Miksis equation[32] which accounts for the liquid compressibility of the first order. Adding p_r as a secondary driving term into the external driving pressure and neglecting coupling terms of higher order[33, 34] lead to the equation of radial motion of bubble 2[35]:

$$\begin{aligned}
&\left(1-\frac{\dot{R}_2}{c}\right)R_2\ddot{R}_2+\left(\frac{3}{2}-\frac{\dot{R}_2}{2c}\right)\dot{R}_2^2\\
&=\frac{1}{\rho}\left(1+\frac{\dot{R}_2}{c}\right)\left[p_2(R_2,\dot{R}_2)-p_0-p_{\mathrm{ex}}(t)\right]\\
&+\frac{\dot{R}_2}{\rho c}\frac{d}{dt}\left[p_2(R_2,\dot{R}_2)-p_{\mathrm{ex}}(t)\right]
\end{aligned}\tag{2}$$

where dots denotes time differentiation, ρ and c are the equilibrium liquid density and the speed of sound of the liquid, p_0 is the hydrostatic pressure in the far field, $p_{\mathrm{ex}}(t)=p_a\sin\omega t$ is the external driving pressure, and $p_2(R_2,\dot{R}_2)$ is the liquid pressure at the bubble wall. It should be noted that the retarded effects in the coupling and driving terms are neglected in Eq. (2)[35].

We assume that the behavior of the gas in the bubble is approximately polytropic and set

$$p_2=\left(p_0+\frac{2S}{R_{20}}\right)\left(\frac{R_{20}}{R_2}\right)^{3\kappa}-\frac{2S}{R_2}-\frac{4\mu\dot{R}_2}{R_2}\tag{3}$$

where R_{20} is the equilibrium radius of bubble 2, S is the surface tension, κ is the polytropic index, and μ is the dynamic liquid viscosity. The equations for bubble 1 is obtained by exchanging the indices 1 and 2 in Eqs. (2) and (3). The adiabatic natural frequency of an uncoupled bubble of R_0 at rest in an unbounded liquid media is

$$\omega_N=\frac{1}{R_0}\left[\frac{3\gamma p_0}{\rho}+\frac{2(3\gamma-1)S}{\rho R_0}\right]^{\frac{1}{2}}\tag{4}$$

where γ is the ratio of specific heats.

2.2. Nondimensional form

In the following perturbation method, it is convenient to nondimensionalize the equations of Substituting $R_1=R_{10}(1+\Delta x)$, $R_2=R_{20}(1+\Delta y)$ and $t=\omega_N^{-1}t^*$, the equations motion of the two bubbles are reduced to

$$\begin{aligned}
\left(1-\frac{\Delta\dot{x}}{C}\right)(1+\Delta x)\,\Delta\ddot{x}+\frac{3}{2}\left(1-\frac{\Delta\dot{x}}{3C}\right)\Delta\dot{x}^2&=\left(1+\frac{\Delta\dot{x}}{C}\right)\left[p_1^*(\Delta x,\Delta\dot{x})-\mathrm{Eu}(1+A^*\sin\omega_f t)\right]\\
&+\frac{\Delta\dot{x}}{C}\frac{d}{dt^*}\left[p_1^*(\Delta x,\Delta\dot{x})-\mathrm{Eu}A^*\sin\omega_f t\right]\\
&-\frac{{R^*}^3}{d^*}\left[(1+\Delta y)^2\Delta\ddot{y}+2\Delta\dot{y}^2(1+\Delta y)\right]
\end{aligned}\tag{5}$$

$$\begin{aligned}
\left(1-\frac{R^*\Delta\dot{y}}{C}\right)(1+\Delta y)\,\Delta\ddot{y}+\frac{3}{2}\left(1-\frac{R^*\Delta\dot{y}}{3C}\right)\Delta\dot{y}^2&=\left(1+\frac{R^*\Delta\dot{y}}{C}\right)\left[p_2^*(\Delta y,\Delta\dot{y})-\frac{\mathrm{Eu}}{{R^*}^2}(1+A^*\sin\omega_f t)\right]\\
&+\frac{R^*\Delta\dot{y}}{C}\frac{d}{dt^*}\left[p_2^*(\Delta y,\Delta\dot{y})-\frac{\mathrm{Eu}}{{R^*}^2}A^*\sin\omega_f t\right]\\
&-\frac{1}{d^*{R^*}^2}\left[(1+\Delta x)^2\Delta\ddot{x}+2\Delta\dot{x}^2(1+\Delta x)\right]
\end{aligned}\tag{6}$$

where Δ symbolizes small perturbation of the corresponding variables, and $p_1^*(\Delta x, \Delta\dot{x})$ and $p_2^*(\Delta y, \Delta\dot{y})$ are the dimensionless liquid pressures at the bubble walls given by

$$p_1^* = \left(\mathrm{Eu} + \frac{2}{\mathrm{We}}\right)\left(\frac{1}{1+\Delta x}\right)^{3\kappa} - \frac{2}{\mathrm{We}}\frac{1}{1+\Delta x} - \frac{4}{\mathrm{Re}}\frac{\Delta\dot{x}}{1+\Delta x}, \tag{7}$$

$$p_2^* = \left(\frac{\mathrm{Eu}}{R^{*2}} + \frac{2R^{*3}}{\mathrm{We}}\right)\left(\frac{1}{1+\Delta y}\right)^{3\kappa} - \frac{2R^{*3}}{\mathrm{We}}\frac{1}{1+\Delta y} - \frac{4R^{*2}}{\mathrm{Re}}\frac{\Delta\dot{y}}{1+\Delta y}. \tag{8}$$

Here, all the dimensionless parameters are defined with respect to R_{10} and ω_N as

$$\begin{aligned} &R^* = \frac{R_{20}}{R_{10}}, \quad d^* = \frac{d}{R_{10}}, \\ &A^* = \frac{p_a}{p_0}, \quad \omega_f = \frac{\omega}{\omega_N}, \quad C = \frac{c}{\omega_N R_{10}}, \\ &\mathrm{Eu} = \frac{p_0}{\rho\omega_N^2 R_{10}^2}, \quad \mathrm{We} = \frac{\rho\omega_N^2 R_{10}^3}{S}, \quad \mathrm{Re} = \frac{\rho\omega_N R_{10}^2}{\mu} \end{aligned} \tag{9}$$

where R^* is the ratio of the initial radii, d^* is the dimensionless separation distance, A^* is the driving pressure normalized by the static pressure in the far field, ω_f is the angular frequency, C is the speed of sound in liquid, and Eu, We and Re are Euler, Weber and Reynolds number, respectively. Since the temporal time is nondimesionalized using the natural frequency of an unbounded bubble ω_N, the order of the velocity and that of the acceleration of the bubble wall do not change after time differentiation if the excitation frequency is near the natural frequency of the bubble ($\omega_f \approx 1$). Therefore, the order of $\Delta\dot{x}$ and that of $\Delta\ddot{x}$ are assumed the same as that of Δx in the primary resonance considered in this study. Throughout the following perturbation analysis, we can assume small amplitude oscillation and set the order of Δx, Δy and their derivatives to be a small but finite dimensionless quantity ϵ.

2.3. Linear normal modes

Linear truncation and dropping the inhomogeneous terms of Eqs. (5) to (8) with respect to Δ leads to

$$\Delta\ddot{x} + c_x\Delta\dot{x} + \omega_x^2\Delta x = -e_x\left(1-\Delta x\right)\sin\omega_f t - \mu_x\Delta\ddot{y} \tag{10}$$

$$\Delta\ddot{y} + c_y\Delta\dot{y} + \omega_y^2\Delta y = -e_y\left(1-\Delta y\right)\sin\omega_f t - \mu_y\Delta\ddot{x} \tag{11}$$

or in a vector form with $\mathbf{x}= (\Delta x, \Delta y)^T$

$$\mathrm{M}\ddot{\mathbf{x}} + \mathrm{C}\dot{\mathbf{x}} + \left(\mathrm{K} - \mathrm{F}\sin\omega_f t\right)\mathbf{x} = \mathbf{0} \tag{12}$$

where ω_i $(i = x, y)$ is the partial natural frequency of the individual bubbles, c_i is the damping coefficient due to the viscous and radiation effects, μ_i is the strength of the acceleration's coupling term which is inversely proportional to the separation distance, and e_i is the driving amplitude of the acoustic pressure. Expressions for these parameters and matrices M, C, K and F are listed in Appendix A. Eq. (12) is a damped Mathieu-type equation driven by a harmonic excitation, and the forth term on the left hand side give rise to parametric instability when the driving amplitude and frequency satisfy specific conditions. However, we can neglect this parametric resonance term in the small amplitude assumption.

In general, a N degrees-of-freedom linear oscillation system can have N natural frequencies and corresponding LNMs which are derived from the eigenvalue problem of $\mathrm{M}^{-1}\mathrm{K}$. We denote by $\omega_{\mathrm{L}1}$ and $\omega_{\mathrm{L}2}$ the modal natural frequencies of the LNMs of the system as

$$\omega_{\mathrm{L}1}^2 = \frac{\omega_x^2 + \omega_y^2 - \sqrt{(\omega_x^2+\omega_y^2)^2 - 4(1-\mu_x\mu_y)\omega_x^2\omega_y^2}}{2(1-\mu_x\mu_y)}, \tag{13}$$

$$\omega_{\mathrm{L}2}^2 = \frac{\omega_x^2 + \omega_y^2 + \sqrt{(\omega_x^2+\omega_y^2)^2 - 4(1-\mu_x\mu_y)\omega_x^2\omega_y^2}}{2(1-\mu_x\mu_y)}. \tag{14}$$

Eqs. (13) and (14) are identical with that of Zabolotsukaya[6] termed as the partial natural frequency in the paper. Particularly for equally-sized two bubbles, the above equations become

$$\omega_{\mathrm{L1}} = \frac{\omega_N}{\sqrt{1+d^{*-1}}}, \tag{15}$$

$$\omega_{\mathrm{L2}} = \frac{\omega_N}{\sqrt{1-d^{*-1}}} \tag{16}$$

whose oscillation are in-phase and out of phase, respectively. The corresponding LNMs are described in Fig. 2, and the nondimensional parameters used are given in Table 1. The LNMs are uniquely specified by the ratio between the inertia and stiffness of the system and invariant with respect to the state of motion. Indeed, L1 and L2 are depicted as a straight vertical line in Fig. 2 which shows that the LNMs are not functions of the oscillation amplitude. What is notable is that the forced oscillation of a two-DoF system has two resonance points in the neighborhood of the LNMs. Therefore, it is worth exploring normal modes and their normal natural frequencies for understanding the global dynamics of coupled oscillating systems. In the next section, we readily extend the concept of LNMs to the nonlinear modal analysis of the two-bubble oscillators.

3. Perturbation analysis

3.1. Small-amplitude approximation

In order to construct perturbative solutions based on a Taylor series expansion, we approximate Eqs. (5) to (8) by truncated equations considering terms to ϵ^3

$$\begin{aligned}&\Delta\ddot{x} + c_x\Delta\dot{x} + \omega_x^2\Delta x = -b\left(1-\Delta x\right)\Delta\dot{x}^2 - \beta_{xx}\Delta x^2 - \beta_{xxx}\Delta x^3 \\ &- e_x\sin\omega_f t - \mu_x\left[\left(1+\Delta y\right)^2\Delta\ddot{y} + \left(1+\Delta y\right)\Delta\dot{y}^2\right]\end{aligned} \tag{17}$$

$$\begin{aligned}&\Delta\ddot{y} + c_y\Delta\dot{y} + \omega_y^2\Delta y = -b\left(1-\Delta y\right)\Delta\dot{y}^2 - \beta_{yy}\Delta y^2 - \beta_{yyy}\Delta y^3 \\ &- e_y\sin\omega_f t - \mu_y\left[\left(1+\Delta x\right)^2\Delta\ddot{x} + \left(1+\Delta x\right)\Delta\dot{x}^2\right]\end{aligned} \tag{18}$$

where β_{xx}, β_{yy}, β_{xxx} and β_{yyy} are parameters associated with the nonlinear terms (See Appendix A). The other parameters associated with the linear terms are the same as Eq. (12) except that $b = 3/2$ is a constant.

For the sake of the perturbation analysis, we assume that damping coefficients c_i and coupling strength μ_i are of the order of $O(\epsilon^2)$, and sound amplitude e_i is of the order of $O(\epsilon^3)$ so that all the terms in Eqs. (17) and (18) are at least of the order of $O(\epsilon^3)$ and set

$$c_i = \epsilon^2\hat{c}_x, \quad \mu_i = \epsilon^2\hat{\mu}_i, \quad e_i = \epsilon^3\hat{e}_i. \tag{19}$$

3.2. Perturbation solution

To obtain the approximate solution of Eqs. (17) and (18), we use the method of multiple scales[23, 36]. Instead of using the driving frequency ω_f as a control parameter, we use a detuning parameter $\sigma = \epsilon^2\hat{\sigma}$ which indicates the deviation of ω_f from ω_x such that

$$\omega_f = \omega_x + \epsilon^2\hat{\sigma} \tag{20}$$

Here, we consider nearly equal-sized bubbles and denote the difference of the natural frequencies of the bubbles by $\alpha = \epsilon^2\hat{\alpha}$ in the form

$$\omega_y = \omega_x + \epsilon^2\hat{\alpha} \tag{21}$$

On the basis of the method of multiple scales, we introduce three time scales $t_0 = t$, $t_1 = \epsilon t$ and $t_2 = \epsilon^2 t$. Accordingly, the total derivative is $d/dt = D_0 + \epsilon D_1 + \epsilon^2 D_2$ where $D_k = \partial/\partial t_k$ denotes partial differentiation

with respect to t_k. The approximate solution of Δx and Δy as functions of these multiple time scales are assumed in the form

$$\Delta x\left(t_0,t_1,t_2\right)=\epsilon x_1+\epsilon^2 x_2+\epsilon^3 x_3+\cdots, \tag{22}$$

$$\Delta y\left(t_0,t_1,t_2\right)=\epsilon y_1+\epsilon^2 y_2+\epsilon^3 y_3+\cdots \tag{23}$$

where successively determined x_i and y_i are the solution of the ϵ^i order. After substituting Eq. (19) to (23) into Eq. (17) and (18) and collecting powers of ϵ, we find following a set of partial differential equations.
$O(\epsilon)$:

$$D_0^2 x_1+\omega_x^2 x_1=0 \tag{24}$$

$$D_0^2 y_1+\omega_x^2 y_1=0 \tag{25}$$

$O(\epsilon^2)$:

$$D_0^2 x_2+\omega_x^2 x_2=-2D_0D_1x_1-b\left(D_0x_1\right)^2-\beta_{xx}x_1^2 \tag{26}$$

$$D_0^2 y_2+\omega_x^2 y_2=-2D_0D_1y_1-b\left(D_0y_1\right)^2-\beta_{yy}y_1^2 \tag{27}$$

$O(\epsilon^3)$:

$$\begin{aligned} D_0^2 x_3+\omega_x^2 x_3=&-D_1^2x_1-2D_0D_2x_1-2D_0D_1x_2\\ &-2b(D_0x_1)(D_1x_1)+2b(D_0x_1)(D_0x_2)+bx_1(D_0x_1)^2\\ &-\hat{c}_xD_0x_1-2\beta_{xx}x_1x_2-\beta_{xxx}x_1^3-\hat{\mu}_xD_0^2y_1-\hat{e}_x\sin\omega_f t^* \end{aligned} \tag{28}$$

$$\begin{aligned} D_0^2 y_3+\omega_x^2 y_3=&-D_1^2y_1-2D_0D_2y_1-2D_0D_1y_2\\ &-2b(D_0y_1)(D_1y_1)+2b(D_0y_1)(D_0y_2)+by_1(D_0y_1)^2\\ &-\hat{c}_yD_0y_1-2\beta_{yy}y_1y_2-\beta_{yyy}y_1^3-\hat{\mu}_yD_0^2x_1-\hat{e}_y\sin\omega_f t^*\\ &-2\omega_x\hat{\alpha}y_1 \end{aligned} \tag{29}$$

The general solutions of Eqs. (24) and (25) are

$$x_1=A_x(t_1,t_2)\mathrm{e}^{i\omega_x t_0}+cc \tag{30}$$

$$y_1=A_y(t_1,t_2)\mathrm{e}^{i\omega_x t_0}+cc \tag{31}$$

where cc stands for the complex conjugate of the preceding terms on the right hand side. Substituting Eqs. (30) and (31) into Eqs. (26) and (27) yields

$$D_0^2 x_2+\omega_x^2 x_2=-2iD_1A_x\mathrm{e}^{i\omega_x t_0}+bA_x^2\mathrm{e}^{2i\omega_x t_0}-\beta_{xx}x_1^2 \tag{32}$$

$$D_0^2 y_2+\omega_x^2 y_2=-2iD_1A_y\mathrm{e}^{i\omega_x t_0}+bA_x^2\mathrm{e}^{2i\omega_x t_0}-\beta_{yy}y_1^2 \tag{33}$$

The first terms on the right hand side of Eqs. (32) and (33) produces secular terms in x_2 and y_2, respectively, which make the solution grow unboundedly in time. To eliminate the secular terms, we exert following solvability conditions:

$$D_1A_x(t_1,t_2)=0 \tag{34}$$

$$D_1A_y(t_1,t_2)=0 \tag{35}$$

Solving Eqs. (34) and (35), A_x and A_y turn out to be only a function of t_2, and the solutions of Eqs. (32) and (33) are

$$x_2=-\frac{\beta_{xx}-b\omega_x}{3\omega_x^2}A_x^2\mathrm{e}^{2i\omega_x t_0}-\frac{\beta_{xx}+b\omega_x^2}{\omega_x^2}|A_x|^2+cc \tag{36}$$

$$y_2=-\frac{\beta_{yy}-b\omega_x}{3\omega_x^2}A_y^2\mathrm{e}^{2i\omega_x t_0}-\frac{\beta_{yy}+b\omega_x^2}{\omega_x^2}|A_y|^2+cc \tag{37}$$

Similarly, substituting Eqs. (30), (31), (36) and (37) into Eqs. (28) and (29) leads to solvability conditions so as to eliminate the secular terms in x_3 and y_3.

$$2i\omega_x D_2 A_x + i\omega_x \hat{c}_x A_x - \omega_x K_x A_x |A_x|^2 - \omega_x^2 \hat{\mu}_x A_x - \frac{i\hat{e}_x}{2} \mathrm{e}^{i\hat{\sigma} t_2} = 0 \tag{38}$$

$$2i\omega_x D_2 A_y + i\omega_x \hat{c}_y A_y - \omega_x K_y A_y |A_y|^2 - \omega_x^2 \hat{\mu}_y A_y - \frac{i\hat{e}_y}{2} \mathrm{e}^{i\hat{\sigma} t_2} + 2\omega_x \hat{\alpha} A_y = 0 \tag{39}$$

where

$$K_x = -\frac{3\beta_{xxx}}{\omega_x} + \frac{10\beta_{xx}^2}{3\omega_x^3} + b\left(\frac{7\omega_x}{3} + \frac{10}{3\omega_x}\right) \tag{40}$$

$$K_y = -\frac{3\beta_{yyy}}{\omega_x} + \frac{10\beta_{yy}^2}{3\omega_x^3} + b\left(\frac{7\omega_x}{3} + \frac{10}{3\omega_x}\right) \tag{41}$$

To solve Eqs. (38) and (39) for A_x and A_y, we transform complex functions A_x and A_y into the polar form

$$\epsilon A_x(t_2) = \frac{1}{2} a_x(t_2) \mathrm{e}^{i[\phi_x(t_2) + \hat{\sigma} t_2]} \tag{42}$$

$$\epsilon A_y(t_2) = \frac{1}{2} a_y(t_2) \mathrm{e}^{i[\phi_y(t_2) + \hat{\sigma} t_2]} \tag{43}$$

where a_x, a_y, ϕ_x and ϕ_y are real functions of t_2. Substituting Eqs. (42) and (43) into Eqs. (38) and (39), and separating the results into the real and imaginary parts, a following set of amplitude equations for the oscillation amplitude and the phase shift are obtained.

$$\frac{da_x}{dt} = -\frac{c_x}{2} a_x + \frac{\omega_x \mu_x}{2} a_y \sin(\phi_y - \phi_x) + \frac{e_x}{2\omega_x} \cos\phi_x \tag{44}$$

$$\frac{d\phi_x}{dt} = -\sigma - \frac{K_x}{8} a_x^2 - \frac{\omega_x \mu_x}{2} \frac{a_y}{a_x} \cos(\phi_y - \phi_x) - \frac{e_x}{2\omega_x a_x} \sin\phi_x \tag{45}$$

$$\frac{da_y}{dt} = -\frac{c_y}{2} a_y + \frac{\omega_x \mu_y}{2} a_x \sin(\phi_x - \phi_y) + \frac{e_y}{2\omega_x} \cos\phi_y \tag{46}$$

$$\frac{d\phi_y}{dt} = -\sigma - \frac{K_y}{8} a_y^2 - \frac{\omega_x \mu_y}{2} \frac{a_x}{a_y} \cos(\phi_x - \phi_y) - \frac{e_y}{2\omega_x a_y} \sin\phi_y + \alpha a_y \tag{47}$$

where the scaled parameters by using ϵ are reset to the original form without ($\hat{}$). Substituting Eqs. (42) and (43) into Eqs. (30) and (31) yields the first approximate solution

$$\Delta x = a_x \cos(\omega_f t + \phi_x) + O(\epsilon^2) \tag{48}$$

$$\Delta y = a_y \cos(\omega_f t + \phi_y) + O(\epsilon^2) \tag{49}$$

3.3. Nonlinear normal modes

In analogy with the LNMs, we consider undamped free oscillation of Eqs. (44) to (47). Setting $c_x = c_y = e_x = e_y = 0$, and removing the driving term, the amplitude equations governing a_i and ϕ_i are rewritten as

$$\frac{da_y}{dt} = \frac{1}{2} \omega_x \mu_x a_y \sin(\phi_y - \phi_x) \tag{50}$$

$$\frac{d\phi_x}{dt} = -\frac{K_x}{8} a_x^2 - \frac{1}{2} \omega_x \mu_x \frac{a_y}{a_x} \cos(\phi_y - \phi_x) \tag{51}$$

$$\frac{da_x}{dt} = \frac{1}{2} \omega_x \mu_y a_x \sin(\phi_x - \phi_y) \tag{52}$$

$$\frac{d\phi_y}{dt} = -\frac{K_y}{8} a_y^2 - \frac{1}{2} \omega_x \mu_y \frac{a_x}{a_y} \cos(\phi_x - \phi_y) + \alpha a_y \tag{53}$$

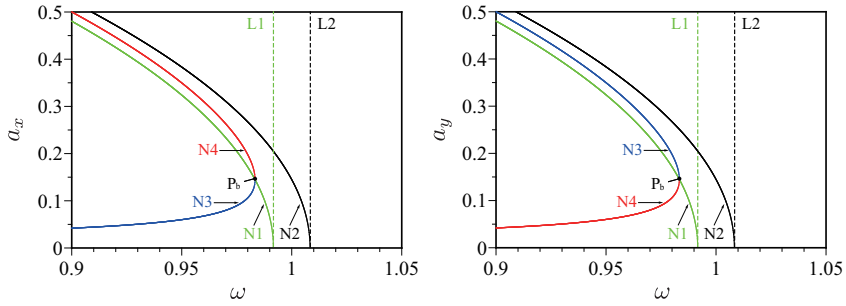

Figure 2: The NNMs Ni ($i = 1, 2, 3, 4$) as a function of normal oscillation frequency ω (Case A: $R_{10} = R_{20} = 10\ \mu m$). The LNMs, L1 and L2, are also shown for comparison.

Recalling the definition of normal modes that motions which depart from a NNM confined in it for all time, we consider the steady-state solution of Eqs. (50) to (53). To obtain explicit expression of the NNMs, letting $da_x/dt = da_y/dt = 0$ in Eqs. (50) and (52) yields

$$\phi_x - \phi_y = 0,\ \pi \tag{54}$$

which correspond to in-phase and out-of-phase NNMs, respectively. Since $d\left(\phi_x - \phi_y\right)/dt = 0$ from Eq. (54), Eqs. (51) and (53) lead to a following nonlinear algebraic relation for a_x and a_y.

$$-\frac{K_x}{8}a_x^2 + \frac{K_y}{8}a_y^2 \mp \frac{\omega_x}{2}\left(\frac{\mu_x a_y}{a_x} - \frac{\mu_y a_x}{a_y}\right) - \alpha a_y = 0 \tag{55}$$

The first approximate solution of the free oscillation is

$$\Delta x = a_x \cos\Omega_x(t) + O(\epsilon^2) \tag{56}$$

$$\Delta y = a_y \cos\Omega_y(t) + O(\epsilon^2) \tag{57}$$

where $\Omega_i(t) = \omega_x t + \phi_i$ is the oscillation phase of the normal mode. The normal frequency of Δx and Δy, denoted by ω_1 and ω_2 are given by

$$\omega_1 \equiv \frac{d\Omega_x(t)}{dt} = \omega_x - \frac{K_x}{8}a_x^2 - \frac{\omega_x \mu_x a_y}{2a_x}\cos\left(\phi_y - \phi_x\right) \tag{58}$$

$$\omega_2 \equiv \frac{d\Omega_y(t)}{dt} = \omega_x - \frac{K_y}{8}a_y^2 - \frac{\omega_x \mu_y a_x}{2a_y}\cos\left(\phi_x - \phi_y\right) + \alpha \tag{59}$$

On the NNMs where a_x and a_y satisfies Eq. (55), the bubbles oscillate at the same frequency ω which are determined by Eq. (58) and (59). In order to complete understanding a bifurcation structure of the normal modes, the case of equally-sized bubbles is considered in the following. In this case the perturbation parameter α vanishes, and we can analytically obtain the oscillation frequency and amplitude at the bifurcation point. Straightforward calculations using the symmetric property of the system and Eq. (55) lead to

$$\left(a_x^2 - a_y^2\right)\left[-\frac{K_x}{8} \pm \frac{\omega_x \mu_x}{2a_x a_y}\right] = 0 \tag{60}$$

where K_y and μ_y are replaced by K_x and μ_x owing to the equality of the bubble sizes. Assuming a_x and a_y to be positive quantities without loss of generality, Eq. (60) produces

$$a_y = \begin{cases} a_x, \dfrac{4\omega_x \mu_x}{K_x a_x} & (\phi_x - \phi_y = 0) \\ a_x & (\phi_x - \phi_y = \pi) \end{cases} \tag{61}$$

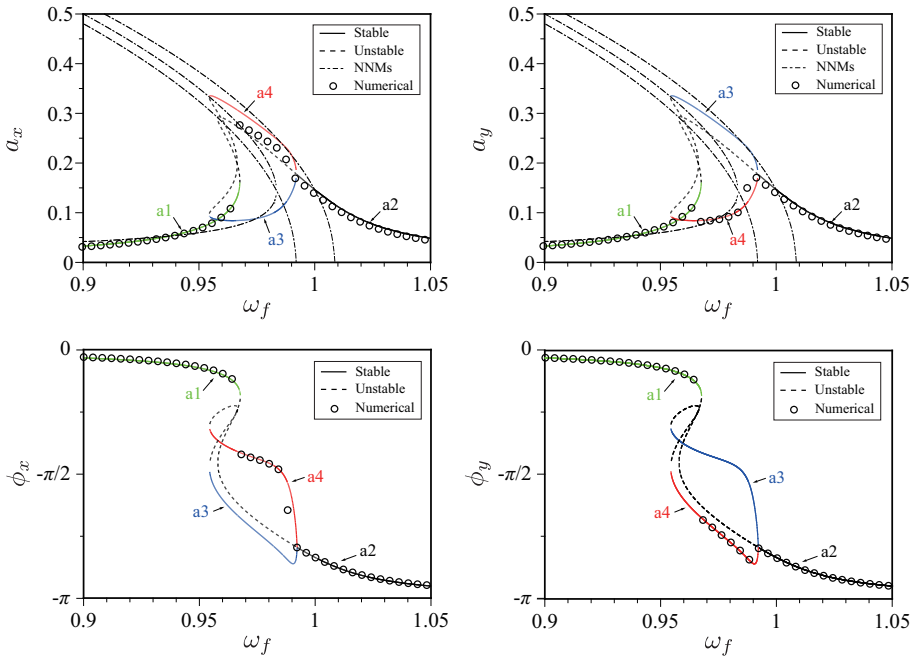

Figure 3: Amplitude (top) and phase shift (bottom) of the steady-state fundamental component for case B as a function of the nondimensional driving frequency denoted by ai ($i = 1, 2, 3, 4$) in different colors. Solid and dashed lines stand for stable and unstable solutions, respectively. For convenience, the NNMs in Fig. 2 are also depicted. The numerical results (circles) are the steady-state fundamental component extracted from the FFT spectrum of time-radius curve.

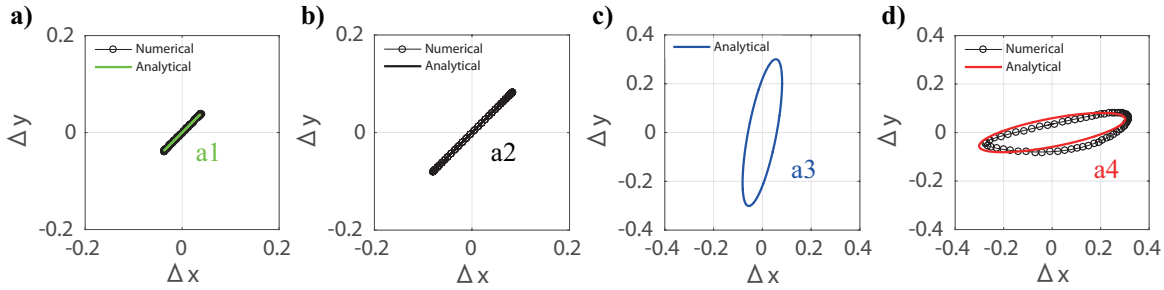

Figure 4: Steady-state solution of the branches a1 to a4 plotted in a Δx-Δy configuration space for (a)the branch a1 at $\omega_f = 0.92$, (b)the branch a2 at $\omega_f = 1.02$, (c)the branch a3 at $\omega_f = 0.97$ and (d)the branch a4 at $\omega_f = 0.97$, The physical parameters are the same as those of Fig. 3. Analytical solutions are the first approximation given by Eqs. (49) and (50). Numerical curves were obtain by time-integration of Eqs. (5) and (6).

Therefore, we obtain four types of NNMs:

N1: $a_x = a_y,\ \phi_x - \phi_y = 0$

N2: $a_x = a_y,\ \phi_x - \phi_y = \pi$

N3: $a_x \geq a_y,\ \phi_x - \phi_y = 0$ (Localized mode)

N4: $a_x \leq a_y,\ \phi_x - \phi_y = 0$ (Localized mode)

where Ni ($i = 1, 2, 3, 4$) denotes a branch of the four types of NNMs. The non-localized normal modes N1 and N2 correspond to in-phase and out-of-phase NNM motions. Localized modes N3 and N4 indicate a localized oscillation where the total vibration energy of the system is not evenly shared between the oscillators, but confined to either one. Fig. 2 illustrates the NNMs as a function of oscillation frequency where the LNMs Li ($i = 1, 2$) are also depicted for comparison. The frequency of N1 and N2 decreases with increasing oscillation amplitude, and they asymptote to their linear counterparts L1 and L2 in the limit of zero-amplitude. The in-phase mode N1 splits up at the bifurcation point $\mathrm{P_b}$, and the localized normal modes N3 and N4 emerge on either sides of N1 as a result of the pitchfork bifurcation. It follows that nonlinear localized resonance

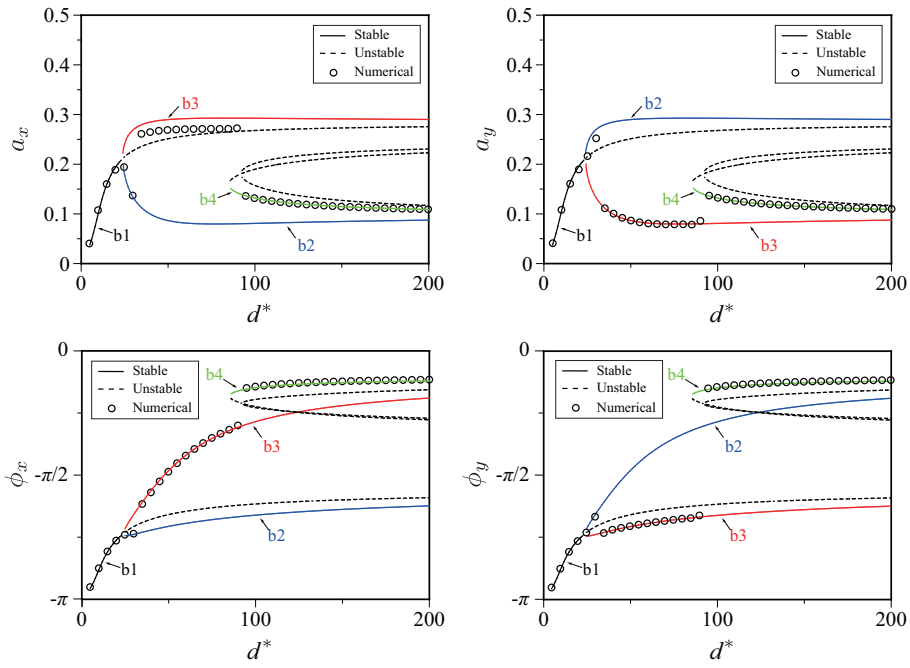

Figure 5: Amplitude (top) and phase shift (bottom) of the steady-state fundamental component for case C as a function of the nondimensional separation distance denoted by bi ($i = 1, 2, 3, 4$) in different colors. Solid and dashed lines stand for stable and unstable solutions, respectively. The numerical results (circles) are the steady-state fundamental component extracted from the FFT spectrum of time-radius curve.

is expected in the neighborhood of the localized NNMs if the vibration amplitude exceeds a certain critical value. What is notable is that nonlinear localization can occur even in an equal-sized pair of bubbles which has no structural detuning but is completly symmetric. The amplitude and the frequency at the bifurcation point, $\mathrm{P_b}$, are given by

$$a_{\mathrm{bp}} = 2\left[\frac{\omega_x \mu_x}{K_x}\right]^{\frac{1}{2}} \tag{62}$$

$$\omega_{\mathrm{bp}} = \omega_x(1-\mu_x) \tag{63}$$

Note that the amplitude at $\mathrm{P_b}$ is proportional to the square root of the ratio between the magnitude of the nonlinearity and radiation coupling. In contrast, the frequency at $\mathrm{P_b}$ is just a linear function of the coupling coefficient. We note that these results are valid only for a limited parameter space with the small-amplitude approximation. Furthermore, the bifurcation structure and their stability highly depend on energy dissipation because the damping effect tends to smooth out the energy localization.

3.4. Steady-state solution

The steady-state amplitude, the phase shift of Δx and Δy and their linear stabilities are shown in Fig. 3 as a function of the driving frequency. The separation distance is fixed to $d^* = 60$, and the driving amplitude is $A^* = 0.0250$. It is clear that the forced oscillation occurs in the neighborhood of the NNMs as is the case with linear resonance. We found that the branch a1 is connected to a saddle-node bifurcation point at its right end, and a supercritical pitchfork bifurcation appears at the left end of a2. Consequently, there is no stable synchronized motion between these two bifurcation points. Instead, the localized solutions a3 and a4 branch out from the pitchfork bifurcation point. We also notice that the localized branch a4 intersects with the non-localized branch a1, and three stable solutions coexist within a narrow range of the driving frequency. Comparison with the numerical results show a good agreement over the range of the parameter limit. In Fig. 4, these four types of steady-state solutions are described in $\Delta x - \Delta y$ configuration space. The non-localized solutions, a1 and a2, look like a straight line with a positive slope of unity in Fig. 4(a) and

Table 1: Dimensionless parameters for air bubbles in water at 298K and the atmospheric ambient pressure. The equilibrium radii of the two bubbles are 10 μm for all the cases. Case A corresponds to an undamped free oscillation (damping and driving pressure are removed), and the other cases are for forced oscillation with damping effects. Note that in case D and E Reynolds number is calculated with the effective kinematic viscosity $\nu_{\text{eff}} = 6.73 \times 10^{-3}$ m^2/s, and the effective polytropic exponent $\kappa_{\text{eff}} = 1.10$. The corresponding driving pressure are 2.5 and 100 kPa for $A^* = 2.50 \times 10^{-2}$ and 1.00, respectively.

Case	R^*	Eu	Re	We	C	Pe	A^*	ω_f	d^*
A	1	0.214	215	64.3	∞	∞	$\cdots$	$\cdots$	60
B	1	0.214	215	64.3	∞	∞	0.0250	0.9-1.1	60
C	1	0.214	215	64.3	∞	∞	0.0250	0.95	5-200
D	1	0.214	215	64.3	11.4	69.5	1.00	0.3-1.1	7.5
E	1	0.214	215	64.3	11.4	69.5	1.00	0.3-1.1	3-45

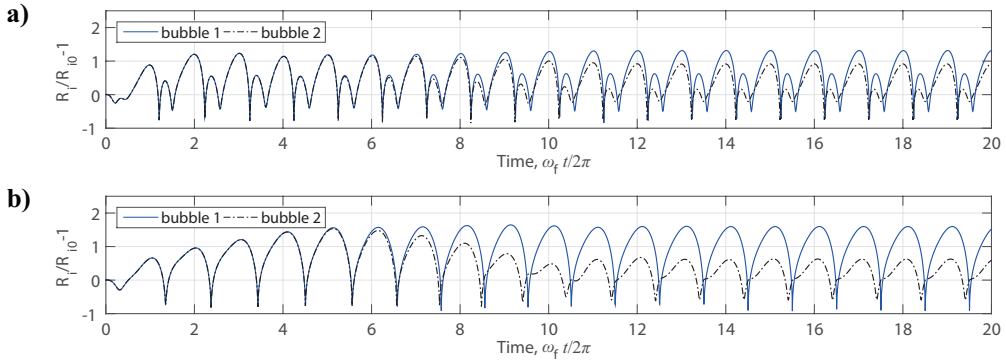

Figure 6: Time-radius curves for $d^* = 7.5$, (a) $\omega_f = 0.40$ (second superharmonic resonance) (b) $\omega_f = 0.70$ (primary resonance).

(b) because of the completely synchronized in-phase motion, while the plot of localized solutions, a3 and a4, are an elongated closed orbit with an oblique axis. The orientation of the axes are due to the localization of the phase difference shown in Fig. 3. The immediate question is to which solution a3 or a4 does the system converge for a typical initial condition. It requires observation of the sensitive dependence of its long-time behavior on initial conditions, which is beyond the scope of this paper. The steady-state amplitude and the phase shift as a function of the separation distance $d^*(= d/R_{10})$ are also shown in Fig. 5 where the driving frequency is fixed to $\omega_f = 0.97$. The similar bifurcation structures (pitchfork and saddle-node bifurcations) are also true as with Fig. 3 for the case of a fixed driving frequency. That is, increasing the separation distance, d^*, brings about multi-valued stable solutions with localized oscillation, leading to a drastic jump phenomenon at about $d^* = 90$ where the phase difference $\phi_y - \phi_x$ changes from $\pi/2$ to zero. It follows that even a small coupling effect exerted from neighboring bubbles are essentially negligible in such nonlinear regime.

4. Numerical results

The preceding weakly nonlinear analysis assumed small-amplitude perturbation and is valid only for the limited parameter space. In this section, large amplitude oscillation for a wide range of the driving frequency and the separation distance as shown in Table 1 are presented. An pair of equally-sized bubbles of 10 μm in radius with a fixed separation distance are driven by a sound pressure amplitude of 100 kPa. We put a small disturbance to the initial radius of bubble 2 in order to avoid a completely symmetric motion, and $(R_1(0), R_2(0), \dot{R}_1(0), \dot{R}_2(0)) = (1, 1.01, 0, 0)$ is used for each ω_f. In addition, we account for the well-known additional damping[27, 28] because the thermal damping dominates over the viscous damping for a resonant

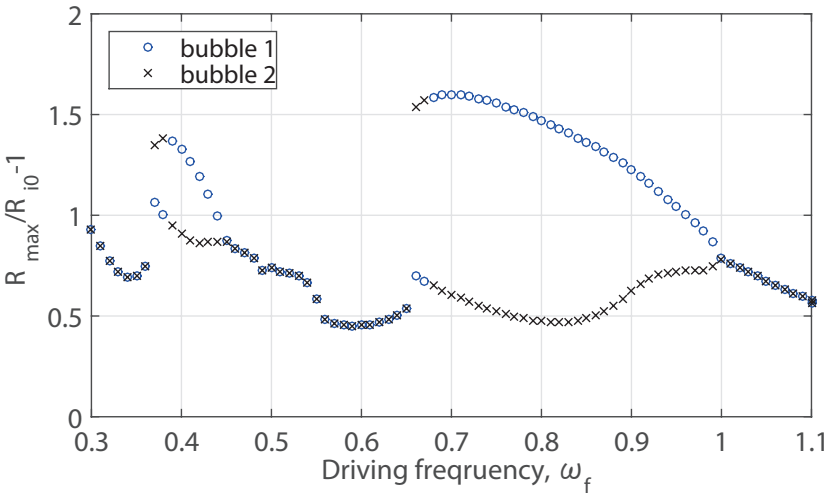

Figure 7: Frequency response curves of the maximum bubble radii obtained from the steady-state oscillation after 32 cycles of the driving period. The physical parameters used are those of case D ($d^* = 7.5$, and $A = 1.00$) in Table 1. The sound pressure corresponds to 100 kPa.

bubble in a wide range of equilibrium bubble sizes. The effective kinematic viscosity ν_{eff} and polytropic index κ_{eff} for thermal behavior of the internal gas are given by a function of Peclet number $\text{Pe} = \omega_f R_{10}^2/\alpha_{\text{th}}$ where α_{th} is the thermal diffusivity of the gas[37]. In the calculation, the governing equation is transformed into a C^∞ equivalent dynamical system[34] to achieve smoother oscillation in the transformed system since a singular behavior due to a violent collapse of a bubble oscillation leads to serious numerical errors. The classical forth order Runge-Kutta method is used for time integration.

In Fig. 6, time-radius curves of typical localized oscillation are plotted for case D with a fixed driving frequency. The oscillation amplitudes are attracted to a localized steady-state values after the transient response decays although both motions of the bubbles look identical during the first eight periods. It is also interesting to note that the phase shifts of the oscillators converge to different values, and the bubbles collapse with a slight time lag. Fig. 7 shows frequency response curves of the maximum bubble radii $R_{i\max}$ obtained from the steady-state oscillation after 32 cycles of the driving period (Case D). The localized oscillation is observed in a wide range of the driving frequency even in the presence of the thermal damping. The magnitudes of $R_{1\max}$ and $R_{2\max}$ are switched around $\omega_f = 0.40$ and 0.70, corresponding to the second superharmonic and primary resonance, respectively. It follows that the magnitude relation of localized oscillation is sensitive, at the vicinity of resonance peaks, to microscopic fluctuation of initial conditions or an external disturbance with the magnitude of no more than 1% of the initial bubble radii.

In order to explore bifurcation structures in $\omega_f - d^*$ space, contour plot of the difference of the maximum amplitude $\Delta R_{\max} = (R_{2\max} - R_{1\max})/R_{10}$ as a function of the driving frequency and the separation distance is illustrated in Fig. 8 where the physical parameters of case E are used. In contrast to the weakly nonlinear case, localization occurs at a short separation distance. This is because both the nonlinearity and coupling strength should be large enough to counterbalance the thermal damping. Therefore, the region of localization shifts toward a low-frequency and short-distance part of the $\omega_f - d^*$ space which is a fairly typical parameter range used in practical experiments and simulations in the early literatures[7, 9, 16, 34, 35, 38]. It follows that even a mono-dispersed bubble cloud can have tremendously complex bifurcation structures depending on its void fraction and the driving pressure amplitude at the nonlinear resonant frequencies.

5. Conclusion

We have provided an asymptotic derivation of the steady-state solutions and underlying NNMs for the primary resonance of two spherical gas bubbles oscillating with a fixed separation distance in order to explore bifurcation structures of the two-bubble oscillators. In the case of equal-sized bubbles of particular interest for this study, an approximate solution of the oscillation amplitude and the phase shift for the fundamental mode bifurcates to produce multi-valued stable solutions in the neighborhood of the NNMs. The distinctive

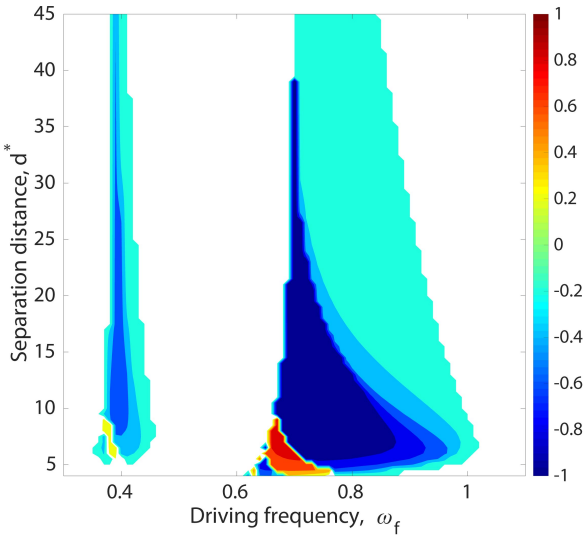

Figure 8: Contour plot of $\Delta R_{\max} = (R_{2\max} - R_{1\max})/R_{10}$ as a function of the driving frequency and the separation distance. Note that $\Delta R_{\max} = 0$ indicates non-localized oscillation which is not plotted, and only localized oscillation $\Delta R_{\max} \neq 0$ is plotted. The physical parameters used are those for case E ($d^* = 3 - 45$, and $A^* = 1.00$) in Table 1.

feature of these solutions is that localized oscillation (localization of vibration energy) can occur depending on the driving frequency and the separation distance between the bubbles, because the identical steady-state motion becomes unstable in a certain range of the parameter space. Requirements necessary for the presence of localized oscillation are summarized as follows. (a) The partial natural frequencies of the individual bubble are close in value so as to evoke the internal resonance. (b) Bubbles are in resonance at the imposed driving frequency. (c) Steady-state oscillation are achieved. (d) The separation distance is within a proper range where the coupling strength counterbalances the nonlinearity of the radial dynamics. (e) Damping effects are not so strong to smooth out the energy distribution among the bubbles. Some of our numerical calculation showed that the localized oscillation occur for a fairly typical parameter range used in practical experiments and simulations in the literature. This makes it almost unfeasible to rigorously describe the bubble cloud dynamics since even a cluster containing a small number of bubbles can have an incomprehensible number of steady-states.

Acknowledgments

We acknowledge Dr. Keita Ando for his comments on the model used in this study. This work is supported by JSPS KAKENHI Grant number No. JP5630079.

Appendix A.

Nondimensional parameters in Eqs. (10) and (11) are

$$\omega_x = \left[3\kappa \mathrm{Eu} + (3\kappa - 1)\frac{2}{\mathrm{We}}\right]^{\frac{1}{2}}, \quad \omega_y = \left[3\kappa \frac{\mathrm{Eu}}{R^{*2}} + (3\kappa - 1)\frac{2R^{*3}}{\mathrm{We}}\right]^{\frac{1}{2}},$$

$$c_x = \frac{4}{\mathrm{Re}} + \frac{\omega_x^2}{\mathrm{M}}, \quad c_y = \frac{4R^{*2}}{\mathrm{Re}} + \frac{\omega_y^2}{R^*\mathrm{M}},$$

$$\mu_x = \frac{R^{*3}}{d^*}, \quad \mu_y = \frac{1}{d^* R^{*2}},$$

$$e_x = \mathrm{Eu}A^*, \quad e_y = \frac{\mathrm{Eu}A^*}{R^{*2}}$$

with which

$$\mathrm{K} = \begin{bmatrix} \omega_x^2 & 0 \\ 0 & \omega_y^2 \end{bmatrix},\ \mathrm{M} = \begin{bmatrix} 1 & \mu_x \\ \mu_y & 1 \end{bmatrix},\ \mathrm{C} = \begin{bmatrix} c_x & 0 \\ 0 & c_y \end{bmatrix},\ \mathrm{F} = \begin{bmatrix} e_x & 0 \\ 0 & e_y \end{bmatrix}.$$

Nondimensional parameters in Eqs. (17) and (18) are

$$\begin{aligned}
\beta_{xx} &= -\frac{(3\kappa+1)(3\kappa+2)-6}{\mathrm{We}} - \frac{(3\kappa+1)(3\kappa+2)-2}{2}\mathrm{Eu}, \\
\beta_{yy} &= -\frac{(3\kappa+1)(3\kappa+2)-6}{\mathrm{We}}R^{*3} - \frac{(3\kappa+1)(3\kappa+2)-2}{2}\frac{\mathrm{Eu}}{R^{*2}}, \\
\beta_{xxx} &= \frac{(3\kappa+1)(3\kappa+2)(3\kappa+3)-24}{3}\frac{1}{\mathrm{We}} - \frac{(3\kappa+1)(3\kappa+2)(3\kappa+3)-6}{6}\mathrm{Eu}, \\
\beta_{yyy} &= \frac{(3\kappa+1)(3\kappa+2)(3\kappa+3)-24}{3}\frac{R^{*3}}{\mathrm{We}} - \frac{(3\kappa+1)(3\kappa+2)(3\kappa+3)-6}{6}\frac{\mathrm{Eu}}{R^{*2}}.
\end{aligned}$$

References

[1] C. E. Brennen, Cavitation and bubble dynamics, Cambridge University Press, 2013.

[2] W. Kim, T.-H. Kim, J. Choi, H.-Y. Kim, Mechanism of particle removal by megasonic waves, Applied Physics Letters 94 (8) (2009) 081908.

[3] M. Emmer, A. Van Wamel, D. E. Goertz, N. De Jong, The onset of microbubble vibration, Ultrasound in medicine & biology 33 (6) (2007) 941–949.

[4] B. L. Helfield, D. E. Goertz, Nonlinear resonance behavior and linear shell estimates for definity and micromarker assessed with acoustic microbubble spectroscopy, The Journal of the Acoustical Society of America 133 (2) (2013) 1158–1168.

[5] C. C. Coussios, R. A. Roy, Applications of acoustics and cavitation to noninvasive therapy and drug delivery, Annu. Rev. Fluid Mech. 40 (2008) 395–420.

[6] E. Zabolotskaya, Interaction of gas-bubbles in a sound field, Soviet Physics Acoustics-Ussr 30 (5) (1984) 365–368.

[7] H. Takahira, T. Akamatsu, S. Fujikawa, Dynamics of a cluster of bubbles in a liquid. theoretical analysis., JSME International Journal Series B Fluids and Thermal Engineering 37 (2) (1994) 297–305.

[8] G. Kerschen, M. Peeters, J.-C. Golinval, A. F. Vakakis, Nonlinear normal modes, part i: A useful framework for the structural dynamicist, Mechanical Systems and Signal Processing 23 (1) (2009) 170–194.

[9] H. Takahira, S. Yamane, T. Akamatsu, Nonlinear oscillations of a cluster of bubbles in a sound field (bifurcation structure), JSME international journal. Series B, fluids and thermal engineering 38 (3) (1995) 432–439.

[10] C. Macdonald, J. Gomatam, Chaotic dynamics of microbubbles in ultrasonic fields, Proceedings of the Institution of Mechanical Engineers, Part C: Journal of Mechanical Engineering Science 220 (3) (2006) 333–343.

[11] K. Chong, C. Quek, F. Dzaharudin, A. Ooi, R. Manasseh, The effects of coupling and bubble size on the dynamical-systems behaviour of a small cluster of microbubbles, Journal of Sound and Vibration 329 (6) (2010) 687–699.

[12] F. Dzaharudin, S. A. Suslov, R. Manasseh, A. Ooi, Effects of coupling, bubble size, and spatial arrangement on chaotic dynamics of microbubble cluster in ultrasonic fields, The Journal of the Acoustical Society of America 134 (5) (2013) 3425–3434.

[13] J. M. Carroll, M. L. Calvisi, L. K. Lauderbaugh, Dynamical analysis of the nonlinear response of ultrasound contrast agent microbubbles, The Journal of the Acoustical Society of America 133 (5) (2013) 2641–2649.

[14] A. F. Vakakis, L. I. Manevitch, Y. V. Mikhlin, V. N. Pilipchuk, A. A. Zevin, Normal Modes and Localization in Nonlinear Systems, John Wiley & Sons, 2008.

[15] T. Ikeda, Y. Harata, K. Nishimura, Intrinsic localized modes of harmonic oscillations in nonlinear oscillator arrays, Journal of Computational and Nonlinear Dynamics 8 (4) (2013) 041009.

[16] A. Ooi, R. Manasseh, Coupled nonlinear oscillations of microbubbles, ANZIAM Journal 46 (2005) 102–116.

[17] R. M. Rosenberg, Normal modes of nonlinear dual-mode systems, Journal of Applied Mechanics 27 (2) (1960) 263–268.

[18] R. M. Rosenberg, The normal modes of nonlinear n-degree-of-freedom systems, Journal of applied Mechanics 29 (1) (1962) 7–14.

[19] R. Rosenberg, On nonlinear vibrations of systems with many degrees of freedom, Advances in applied mechanics 9 (1966) 155.

[20] A. Prosperetti, Nonlinear oscillations of gas bubbles in liquids: steady-state solutions, The Journal of the Acoustical Society of America 56 (3) (1974) 878–885.

[21] A. Francescutto, R. Nabergoj, Steady-state oscillations of gas bubbles in liquids: Explicit formulas for frequency response curves, The Journal of the Acoustical Society of America 73 (2) (1983) 457–460.

[22] X. Li, J. Ji, C. H. Hansen, Non-linear normal modes and their bifurcation of a two dof system with quadratic and cubic non-linearity, International Journal of Non-Linear Mechanics 41 (9) (2006) 1028–1038.

[23] A. H. Nayfeh, D. T. Mook, Nonlinear oscillations, John Wiley & Sons, 2008.

[24] T. Barbat, N. Ashgriz, C.-S. Liu, Dynamics of two interacting bubbles in an acoustic field, Journal of Fluid Mechanics 389 (1999) 137–168.

[25] N. Bremond, M. Arora, C.-D. Ohl, D. Lohse, Controlled multibubble surface cavitation, Physical review letters 96 (22) (2006) 224501.
[26] N. Bremond, M. Arora, S. M. Dammer, D. Lohse, Interaction of cavitation bubbles on a wall, Physics of Fluids (1994-present) 18 (12) (2006) 121505.
[27] C. Devin Jr, Survey of thermal, radiation, and viscous damping of pulsating air bubbles in water, The Journal of the Acoustical Society of America 31 (12) (1959) 1654–1667.
[28] R. B. Chapman, M. S. Plesset, Thermal effects in the free oscillation of gas bubbles, Journal of Basic Engineering 93 (3) (1971) 373–376.
[29] S. Hilgenfeldt, D. Lohse, M. P. Brenner, Phase diagrams for sonoluminescing bubbles, Physics of Fluids (1994-present) 8 (11) (1996) 2808–2826.
[30] C. E. Brennen, Fission of collapsing cavitation bubbles, Journal of Fluid Mechanics 472 (2002) 153–166.
[31] A. Eller, H. Flynn, Rectified diffusion during nonlinear pulsations of cavitation bubbles, The Journal of the Acoustical Society of America 37 (3) (1965) 493–503.
[32] J. B. Keller, M. Miksis, Bubble oscillations of large amplitude, The Journal of the Acoustical Society of America 68 (2) (1980) 628–633.
[33] A. Prosperetti, A. Lezzi, Bubble dynamics in a compressible liquid. part 1. first-order theory, Journal of Fluid Mechanics 168 (1986) 457–478.
[34] U. Parlitz, V. Englisch, C. Scheffczyk, W. Lauterborn, Bifurcation structure of bubble oscillators, The Journal of the Acoustical Society of America 88 (2) (1990) 1061–1077.
[35] R. Mettin, I. Akhatov, U. Parlitz, C. Ohl, W. Lauterborn, Bjerknes forces between small cavitation bubbles in a strong acoustic field, Physical review E 56 (3) (1997) 2924.
[36] A. H. Nayfeh, Perturbation methods, John Wiley & Sons, 2008.
[37] A. Prosperetti, L. A. Crum, K. W. Commander, Nonlinear bubble dynamics, The Journal of the Acoustical Society of America 83 (2) (1988) 502–514.
[38] W. Wiedemair, Z. Tukovic, H. Jasak, D. Poulikakos, V. Kurtcuoglu, Modeling the interaction of microbubbles: Effects of proximity, confinement, and excitation amplitude, Physics of Fluids (1994-present) 26 (6) (2014) 062106.